Second International Conference on **S**ignals **S**ystems **D**ecision and Information Technology **SSD'03**
March 26-28, 2003 – Sousse, Tunisia

Control of a Haptic 3-D Parallel Robot for Virtual Reality

M. Karkoub
Institut National de Recherche Informatique et Automatique (INRIA). Domaine de Voluceau, 78153 Le Chesnay , France.

M.G. Her
Mechanical Engineering Department. Tatung University, 40 Chung-Sang North Rd. 3 rd. Sec., Taipei, Taiwan 10451, ROC

N. M'Sirdi
Université de Versailles St. Quentin (UVSQ) LRV, 10 Avenue de l'Europe, 78140 Vélizy, France

K-S. Hsu
Mechanical Engineering Department. Tatung University, 40 Chung-Sang North Rd. 3 rd. Sec., Taipei, Taiwan 10451, ROC

Abstract

This paper explores the use of a new type of 3-D parallel robot manipulator interface in virtual reality (VR). A parallel motion control of a platform manipulator actuated by three AC servomotors is presented in this paper. A primary stabilizing controller is used to operate the haptic interface device where a realistic simulation of the dynamic interaction forces between a human operator and the simulated virtual object/mechanism is required. Experiments on cutting virtual clay are used to validate the theoretical developments. It was shown that the experimental and theoretical results are in good agreement.

Key Words: *Clay cutting, haptic virtual system, parallel mechanism.*

1. Introduction

VR applications are increasingly spreading and that is due to many factors the most important of which are the evolvement of speed and decreasing cost of computer systems [1]. For example, in the aviation industry, VR is used to train pilots without having to use real planes or risking their lives [2,3]. In almost all VR applications, the human interface plays a crucial role in the success of the system. While using a haptic VR system, the user is immersed and interacting with a simulated environment [4,5,6]. The interaction between the operator and machines is achieved through an intermediary device known as "haptic device". These haptic devices come in many sizes and shapes. Small interface arrangements have been used to simulate surgical tools [7]. Other haptic devices use specialized robot manipulators to apply force feedback between the user and the VR environment [8]. Kazerooni and Her [9] used a haptic interface device for a manpower amplifier. Other realized a tele -operation for a VR system with haptic characteristics allowing the operator to probe and feel a remote virtual environment [10,11]. Kanai and Takahashi [12] developed a model for a haptic interface device which can give the operator a feel that s/he is maneuvering a mass, or pushing onto a spring or a damper. This paper deals with the design, modeling, and control of a virtual reality system with a haptic interface device. The system, which includes the operator arm dynamics, is used to perform a cutting procedure on a virtual clay enabling the operator to feel the interaction force from the virtual environment just as s/he would from a real environment.

2. Kinematics and Inverse Kinematics

First, let us define two coordinate systems: a fixed reference frame *O-XYZ* attached to the base of the mechanism, and a moving coordinate system *O′-X′Y′Z′* attached to the platform (see Figures 1 and 2). Point *O* is located at the center of the base. The points of attachment of the actuated arms to the base are defined as O_j, with *j=1,2,3* and the points of attachment of all follower rods to the platform are defined as P_i, with *i=1,..,6.* To derive the inverse kinematics of the parallel mechanism, a geometric vector is used. Let the coordinates of point P_i in the moving frame, *O′-X′Y′Z′*, be $\{a_i,b_i,c_i\}$ and the coordinates of point O_i in the fixed frame, *O-XYZ*, be $\{x_{i0}, y_{i0}, z_{i0}\}$. Let, $\boldsymbol{P_i}$ be the position vector of point P_i expressed in the fixed coordinate frame; $\boldsymbol{P_i'}$ be the position vector of point P_i expressed in the moving coordinate frame *O′- X′Y′Z′*; and $\boldsymbol{P}$ be the position vector of point *O′* expressed in the fixed frame *O-XYZ* (see Figures 1 and 2). Therefore,

$$\boldsymbol{P_i} = \boldsymbol{P} + \boldsymbol{Q} \times \boldsymbol{P_i'} \qquad \text{for } i=1,\ldots,6 \qquad (1)$$

where $\boldsymbol{Q}$ is the rotation matrix corresponding to the orientation of the platform of the mechanism with respect to the base coordinate frame. The point O_i' is defined as the center of the universal joint connecting the two moving links of the i[th] actuated rod. Moreover, the Cartesian coordinates of point O_i' expressed in the fixed coordinate frame are noted as $\{x_{i1}, y_{i1}, z_{i1}\}$ (see Figures 1 and 2). Therefore, one can write:

$$x_{i1} = x_{i0} + l_{i1} \times \cos\rho_i \times \cos\gamma_i \qquad (2)$$

$$y_{i1} = y_{i0} + l_{i1} \times \cos\rho_i \times \sin\gamma_i \qquad (3)$$

$$z_{i1} = z_{i0} + l_{i1} \times \sin\rho_i \qquad (4)$$

where γ_i is the angle between the *x*-axis of the base coordinate frame and the axis of i[th] actuated joint, ρ_i is the joint variable associated with the i[th] actuated arm, and l_{i1} is the length of the first link of the i[th] actuated arm. From the geometry of the mechanism, one can write,

$$(x_i - x_{i1})^2 + (y_i - y_{i1})^2 + (z_i - z_{i1})^2 = l_{i2}^2 \quad \text{for } i=1,\ldots,6 \qquad (5)$$

Substituting (1)-(4) into (5), leads to:

$$R_i \times \cos\rho_i + S_i \times \sin\rho_i = T_i \qquad (6)$$

$$R_i = (y_i - y_{i0}) \times \cos\gamma_i + (x_i - x_{i0}) \times \sin\gamma_i \qquad (7)$$

$$S_i = z_i - z_{i0} \qquad (8)$$

$$T_i = \frac{(x_i - x_{i0})^2 + (y_i - y_{i0})^2 + (z_i - z_{i0})^2 + l_{i1}^2 - l_{i2}^2}{2l_{i1}} \qquad (9)$$

Further manipulation of (6)-(9) results in

$$\sin\rho_i = \frac{S_i T_i + K_i R_i \sqrt{V_i}}{R_i^2 + S_i^2} \quad \text{for } i=1,\ldots,6 \qquad (10)$$

$$\cos\rho_i = \frac{R_i T_i - K_i S_i \sqrt{V_i}}{R_i^2 + S_i^2} \quad \text{for } i=1,\ldots,6 \qquad (11)$$

$$K_i = \pm 1 \quad V_i = R_i^2 + S_i^2 - T_i^2 \quad \text{for } i=1,\ldots,6 \qquad (12)$$

Since two solutions are obtained for each ρ_i, it is clear that the inverse kinematics problem of this mechanism leads to 8 solutions, which can be distinguished by using branch indices K_i. The velocity equations of the mechanism are needed for the kinematic analysis. Indeed, since the velocity equations represent the linear mapping between the joint velocities and the cartesian velocities, they characterize the kinematic accuracy of a mechanism and they allow the determination of the singularities.

Differentiating (6)-(9) and expanding leads to

$$B_r \times \dot{\theta} = K_r \times \dot{X} \qquad (13)$$

where

$$\dot{\theta} = \begin{bmatrix} \dot{\rho}_1 & \dot{\rho}_2 & \dot{\rho}_3 \end{bmatrix}^T \quad \text{and} \quad \dot{X} = \begin{bmatrix} \dot{x} & \dot{y} & \dot{z} \end{bmatrix}^T$$

or,

$$\dot{X} = K_r^{-1} B_r \dot{\theta} \qquad (14)$$

Equation (13) defines the velocities of the parallel mechanism. The corresponding Jacobian matrix is given by:

$$J = K_r^{-1} B_r \qquad (15)$$

3. The haptic VR Simulation System

A parallel mechanism shown in Fig. 3 was developed to simulate the tele-presence of the clay cutting system with haptic property and its control block diagrams are shown in Figures 4 and 5. The tele-presence with haptic

properties consists of a two-degree-of-freedom *x*-*y* type active handle and the computer interface which simulates the dynamics of the cutting clay system and the environment. The corresponding transfer functions are given by

$$f_h = u_h - T_h y_h , \tag{16}$$

$$y_h = G_h v_h + S_h f_h , \tag{17}$$

where y_h, u_h, and f_h are the handle position, the force imposed on the force sensor supplied by the operator arm, the force imposed on the handle actuator and fed forward to the virtual side of the system, respectively. Moreover, G_h is the transfer function of the active handle actuator, and S_h is the transfer function from f_h to y_h. From Fig. 4, and particularly, the virtual side, the following relationships are obtained:

$$f_t = u_t - T_t y_t , \tag{18}$$

and

$$y_t = G_t v_t + S_t f_t , \tag{19}$$

where y_t, u_t, and f_t are the cutting tool position, the environment force, the force imposed on the cutting tool actuator and fed back to the physical side of the system, respectively. Further, G_t denotes the transfer function of the virtual cutting tool actuator, and S_t the transfer function from f_t to y_t. The dynamics of the cutting tool actuator including the VR system environment can be taken as:

$$G_t = \frac{1}{M_t s^2 + B_t s + K_t} \tag{20}$$

where M_t, B_t and K_t are the virtual cutting tool mass, the coefficient of viscous damping, and the stiffness of the spring, which is related to the modulus of elasticity of the material, respectively. The cutting tool actuator will drive the tool back and forth and finally towards the desired position where the human operator wants by way of maneuvering the handle.

4. Controller Design and Stability Analysis

The control design block diagram is shown in Figs. 4 and 5. Since there is cross-feedback positions and forces between the physical and virtual sides, the operator can feel the reaction force between the cutting tool and the virtual clay system. By properly selecting the compensators C_{h1}, C_{h2}, C_{t1} and C_{t2} the operator can feel the amount of necessary feedback force and move the handle appropriately towards the desired position during the cutting process. Next, a relationship between the output positions of the handle and the cutting tool of the VR system will be established. From Fig. 4, the control signals of the handle and the cutting tool actuators can be written as follows:

$$v_h = C_{h1} f_h - C_{t1} f_t , \tag{21}$$

$$v_t = -C_{h2} f_h + C_{t2} f_t , \tag{22}$$

Hence, the respective outputs of the positions for the handle and the cutting tool can be written as:

$$y_h = G_h \left(C_{h1} f_h - C_{t1} f_t \right) + S_h f_h , \tag{23}$$

$$y_t = G_t \left(- C_{h2} f_h + C_{t2} f_t \right) + S_t f_t . \tag{24}$$

It can be shown that there exists a matrix A_{h1} such that the following is true

$$G_t C_{h2} = A_{h1} \left(G_h C_{h1} + S_h \right), \tag{25}$$

$$G_t C_{t2} + S_t = A_{h1} \left(- G_h C_{t1} \right). \tag{26}$$

From (23) and (24)

$$y_t = A_{h1} y_h , \tag{27}$$

where the elements of the diagonal matrix A_{h1} denote the ratios of the positions of the handle and the cutting tool in the *x*- and *y*-directions, respectively. Next, one can show that the net force imposed by the operator on the cutting tool is given by:

$$f_t = \left(I + T_t G_t C_{t2} + S_h T_t \right)^{-1} \left(G_t T_t C_{h2} \right) f_h \tag{28}$$

$$= \left(C_{t1} G_h \right)^{-1} \left(C_{h1} G_h + S_h \right) f_h^e = A_{h2} f_h^e , \tag{29}$$

where the elements of the diagonal matrix A_{h2} denote the respective ratios of the forces between the handle and the

cutting tool in the x- and y-directions. If A_{h2} and C_{h1} are selected properly, C_{t1} can be obtained as:

$$C_{t1} = (G_h C_{h1} + S_h)(G_h A_{h2})^{-1} \quad (30)$$

and

$$C_{h2} = (-G_t)^{-1} A_{h1}(G_h C_{h1} + S_h), \quad (31)$$

$$C_{t2} = G_t^{-1}(-A_{h1}A_{h2}^{-1}(G_h C_{h1} + S_h) - S_t), \quad (32)$$

Hence, we should select the compensators C_{h1}, C_{h2}, C_{t1} and C_{t2} properly such that the closed-loop VR system is guaranteed to be stable. A sufficient stability condition will be derived using the Nyquist theorem for the closed-loop system.

It can be shown that for the haptic VR system to be stable

1. $I + RGC + RS$ is analytic in RHP;
2. $I + RGC + RS$ has a proper stable inverse transfer function.

or

$$inf_{\omega\in[0,\infty)} \|I + RGC + RS\| > 0 . \quad (33)$$

Since the motion of the *x*-*y* type active handle and the cutting tool are independent in the *x*- and *y*-directions, then, $G_h = diag\{G_{hx}, G_{hy}\}$, $G_t = diag\{G_{tx}, G_{ty}\}$, $S_h = diag\{S_{hx}, S_{hy}\}$, $S_t = diag\{S_{tx}, S_{ty}\}$, $T_h = diag\{T_{hx}, T_{hy}\}$, and $T_t = diag\{T_{tx}, T_{ty}\}$.

For simplicity and no loss of generality, only the motion in the *x*-direction is considered. Similar, conditions can be derived for the motion in the other direction. It can be shown that for achieving the stability of the closed-loop system in the *x*-direction, the following condition has to be met,

$$|G_{hx}C_{h1}| < \left|S_{hx} + (A_{h1}A_{h2}^{-1}T_{tx} + T_{hx})^{-1}\right|, \quad (34)$$

$\forall \omega \in [0,\infty)$,

By proper selection of C_{h1}, the stability margin of the system can be obtained if A_{h1}, A_{h2}, T_t and T_h on the right side of inequality (34) are known *a priori*.

4. Experimental Results

The layout of the experimental setup of the VR system for simulating the cutting clay system, the environment, and the handle is shown in Figure 6. The VR system consists of four components: user interface, networking, simulation, and robot control scheme. The compounded handle actuator and the operator dynamics for the *x*- and *y*-directions are obtained and identified as:

$$G_{hx} = \frac{18s + 1}{0.005s^3 + 0.4s^2 + 18s + 1} \quad (35)$$

and

$$G_{hy} = \frac{8s + 1}{0.002s^3 + 0.17s^2 + 8s + 1} \quad (36)$$

Due to small lead angle of the lead-screw mechanism, the *x*-*y* type active handle used here is a non-back-drivable mechanism, that is, the mechanism has large transmission rate and S_h and S_t are selected as zero. The operator arm dynamics in the x-direction is identified as:

$$T_{hx} = 0.25s^2 + 2s + 6 \ \ (N/m) \quad (37)$$

To show the validity of the proposed control design, an experiment cutting a varying volume virtual clay is performed. The results show that he velocity is constant in the ranges of 3 cm to 6 cm, 6 cm to 9 cm, and 9 cm to 12 cm. However, the value of the velocity is not the same in the three mentioned ranges. The value of the velocity decreases as the operator cuts deeper into the workpiece. This is expected since the value of the viscous damping increases with depth.

Concluding Remarks

In this paper, we have presented a VR system with haptic property to simulate the cutting clay system. The main components of the system include user interface, networking system, a simulated environment, and robot control scheme. The control scheme incorporates the

dynamics of the human arm, actuators, and the virtual environment in the closed-loop control system for stability analysis. An experiment for cutting variable oil clay using the designed VR system is performed. It was shown that the experimental and theoretical results are in good agreement.

Reference

1. Boman, D.K., 1995, "International survey: Virtual-environment research," IEEE Computer, vol. 28, pp. 57-65.

2. Kwon, D.S., Woo, K.Y. and Cho, H.S., 1999, "Haptic Control of the master Hand Controller for a Microsurgical Tele-robot System," Proc. of the 1999 IEEE Int. Conf. on Robotics and Automation.

3. Hannaford, B., 1989, "A design framework for tele-operators with kinematic feedback," IEEE Trans. Robotics and Automation, vol. 5, No. 4.

4. Kazerooni, H., Snyder, T.J., 1995, "Case study on haptic device: human-induced instability in power hand controllers, " J. of Dynamic Systems, Measurement and Control, Vol. 18, No. 1, pp. 7-22.

5. Takahashi, T. and Ogata, H., 1994, "Generating and re-planning robot commands based on human operation," Journal of JSAI, Vol. 8, No. 4, pp. 448-455.

6. Hirata, Y. and Sato, M., 1992, "3-Dimensional interface device for virtual work space," Proc. of the IEEE/RSJ Int. Conf. on Intelligent Robots and Systems, Raleigh, NC, USA, pp. 889-896.

7. Lee, S., Bekey, B., and Bejczy, A.K., 1985, "Computer control of space-borne a tele-operator with sensory feedback," Proc. of the 1985 IEEE Int. Conf. on Robotics and Automation, pp. 205-214.

8. Satoshi, K., and Hidetomo, T., 1996, "Modeling and NC programming for free-form surfaces by haptic interfaces," The 1996 ASME Design Engineering Technical Conference, Irvine, California, August 1996.

9. Minsky, M., Ouh-young, M., 1990, "Feeling and seeing: issues in force display," Computer Graph, Vol. 24, No. 2, pp. 235-243.

10. Reznik, D. and Laugier, C., 1996, "Dynamic simulation and virtual control of a deformable fingertip," IEEE Int. Conf. Robotics Automation, Minneapolis, MN, pp. 1669-1674.

11. Hannaford, B. and Ryu, J-H., 2002, "Time-domain passivity control of haptic interfaces," IEEE Transactions on Robotics and Automation, Vol. 18, No. 1, pp.1-10.

12. Adams, R. and Hannaford, 2002, "Control law design for haptic interfaces to virtual reality," IEEE Transactions on Control Systems Technology, Vol. 10, No. 1, pp. 3-13.

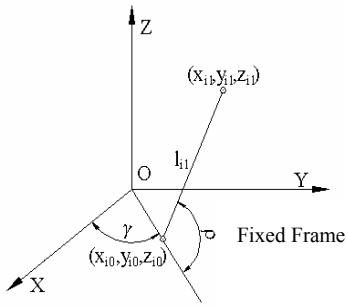

Figure 1. The symbol mark of the actuated arm system.

setup.

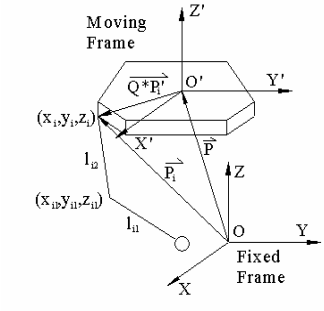

Figure 2. The symbol mark of the inverse kinematics.

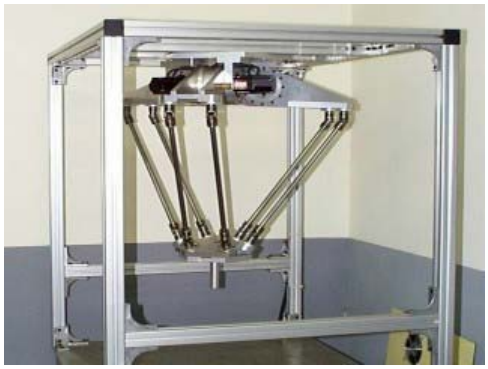

Figure 3. A haptic VR system with parallel active handle: experimental

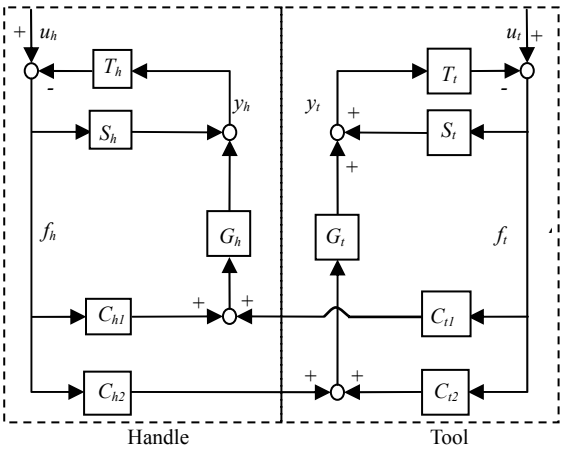

Figure 4. The diagram of the VR system with handle and tool sides.

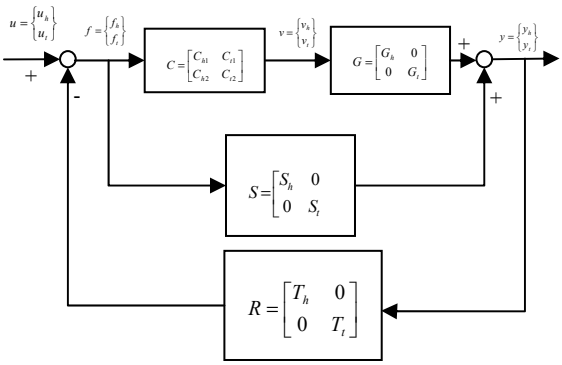

Figure 5. Control design block diagram for the haptic VR system

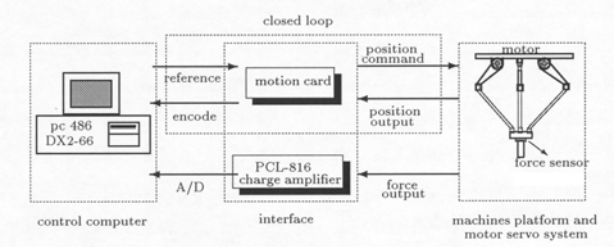

Figure 6. Layout of the experimental setup.

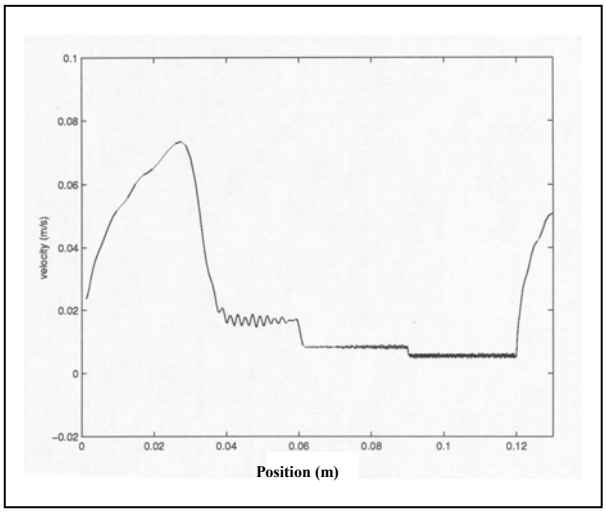

Figure 7. Response of the cutting velocity versus position for variable volume material removal